

# Domain walls and ferroelectric reversal in corundum derivatives

Meng Ye<sup>1,2,\*</sup> and David Vanderbilt<sup>1</sup>

<sup>1</sup>*Department of Physics & Astronomy, Rutgers University, Piscataway, New Jersey 08854, USA*

<sup>2</sup>*The Institute for Molecular Engineering, The University of Chicago, Chicago, Illinois 60637, USA*

(Dated: February 16, 2022)

Domain walls are the topological defects that mediate polarization reversal in ferroelectrics, and they may exhibit quite different geometric and electronic structures compared to the bulk. Therefore, a detailed atomic-scale understanding of the static and dynamic properties of domain walls is of pressing interest. In this work, we use first-principles methods to study the structures of  $180^\circ$  domain walls, both in their relaxed state and along the ferroelectric reversal pathway, in ferroelectrics belonging to the family of corundum derivatives. Our calculations predict their orientation, formation energy, and migration energy, and also identify important couplings between polarization, magnetization, and chirality at the domain walls. Finally, we point out a strong empirical correlation between the height of the domain-wall mediated polarization reversal barrier and the local bonding environment of the mobile  $A$  cations as measured by bond valence sums. Our results thus provide both theoretical and empirical guidance to future searches for ferroelectric candidates in materials of the corundum derivative family.

## I. INTRODUCTION

Ferroelectrics (FEs) are materials with a spontaneous electric polarization that can be reversed by an external electric field.<sup>1</sup> Because the polarization in FEs couples to strains and temperature gradients as well as electric fields, FEs have broad potential applications and are already commonly used in sensor<sup>2</sup> and memory<sup>3</sup> applications. In these materials, regions of different polarization orientation, known as FE domains, often coexist, and the interface between two FE domains is referred to as a domain wall (DW). The hysteresis observed during the switching of FE materials is caused by the nucleation and growth or shrinkage of domains through the motion of DWs in response to an applied electric field favoring one type of domain over the other. To complicate matters, defects can be attracted to the DW and contribute to pinning of the DW motion.<sup>4</sup>

DWs can be seen as topological defects which have different geometric and electronic structures compared to the bulk, so DWs may exhibit rich physics that is not present in the bulk. For instance, in  $\text{BiFeO}_3$ , experiments have shown that the DWs behave as conductive channels in the otherwise insulating background.<sup>5</sup> The same DWs are suggested to exhibit photovoltaic properties as well.<sup>6</sup> Furthermore, it has recently been observed that charged FE DWs, which are energetically unfavorable in general, are abundant in hybrid improper FEs  $(\text{Ca}, \text{Sr})_3\text{Ti}_2\text{O}_7$ .<sup>7</sup> Moreover, in hexagonal manganite  $\text{YMnO}_3$ , the FE DWs form topologically protected vortices,<sup>8</sup> and alternating magnetic moments are found at the FE DW around the vortex core.<sup>9</sup> In addition, the FE DWs are also observed interlocking with chiral DWs in  $\text{Ni}_3\text{TeO}_6$ .<sup>10</sup>

Recently, attention has been drawn to a family of polar materials that can be regarded as derivatives of the corundum  $\text{A}_2\text{O}_3$  structure but with cation ordering on the  $A$  site. The best-known examples are the binary-cation materials  $\text{LiNbO}_3$  and  $\text{LiTaO}_3$ , belonging to the general formula  $\text{ABO}_3$ , but ternary-cation  $\text{A}_2\text{BB}'\text{O}_6$  are

also under investigation.<sup>11</sup> However, polar insulators are not necessarily FE; they can only be considered as such if their polarization can be reversed by an electric field. For example, wurtzite oxides such as  $\text{ZnO}$  are polar, but undergo dielectric breakdown well before polarization reversal can occur. Unfortunately, many of the newly proposed  $\text{ABO}_3$  and  $\text{A}_2\text{BB}'\text{O}_6$  materials are the result of high-pressure syntheses and are only available as powder samples, so that it remains unclear whether or not they would be FE in single-crystal or thin-film form.

Thus, until the experimental growth of single crystals and subsequent observation of domain wall motion can be achieved, theory can play an important role in identifying which materials are most likely to be switchable. We previously carried out first-principles calculations of coherent bulk switching in this class of materials,<sup>11</sup> but did not consider DW-mediated mechanisms. As the DW structure is very different from the bulk, it is interesting to investigate how the DW structure would influence the reversal barrier. The physics of DWs in the corundum derivatives is especially rich because some of these materials are chiral, some are magnetically ordered, and some are both. As a result, the distinct structure at the DW can have additional degrees of freedom that may lead to unique interactions between chiral and FE domains and magnetoelectric effects.

In this work, we use first-principles methods to study the formation and motion of FE DWs at the atomic scale in order to characterize their intrinsic properties and their role in the FE reversal process. The FE candidates that we consider are  $\text{LiNbO}_3$  (LNO),  $\text{LiTaO}_3$ ,  $\text{ZnSnO}_3$ ,  $\text{FeTiO}_3$ ,  $\text{MnTiO}_3$ ,  $\text{Li}_2\text{ZrTeO}_6$ ,  $\text{Li}_2\text{HfTeO}_6$ , and  $\text{Mn}_3\text{WO}_6$ . Our study of the  $180^\circ$  charge-neutral DWs predicts not only the energy and preferred orientation of static DWs, but also the migration path and energy barrier for displacement of a domain wall by a lattice vector during domain reversal. In the case of ferrimagnetic  $\text{Mn}_3\text{WO}_6$ , our DW formation energy results also suggest that FE DWs are simultaneously magnetic DWs,

potentially giving rise to a strong extrinsic magnetoelectric coupling through DW motion. Finally, our results allow us to clarify how the DW-mediated reversal barrier is strongly correlated with the local bonding environment of the  $A$  cations as measured by bond valence sums.

The paper is organized as follows. Sec. II presents a brief summary of our first-principles methods. In Sec. IIIA we explain the principles and assumptions behind our construction of DWs, while the structures and energies of DWs with different orientations are discussed in Sec. IIIB. In Sec. IIIC we consider different magnetic structures at the DWs, leading to the discovery of a potential DW-mediated magnetoelectric coupling in ferromagnetic  $\text{Mn}_3\text{WO}_6$ . Finally, in Sec. IIID we use a structural constraint method to study the migration path and barrier energy in the DW-mediated polarization reversal process, and find a strong correlation between the barrier energy and the local bonding environment of the  $A$  cations. A brief summary is given in Sec. IV.

## II. FIRST-PRINCIPLES METHODS

The calculations are performed with plane-wave density functional theory (DFT) implemented in VASP<sup>12</sup> with PBEsol<sup>13</sup> as the exchange-correlation functional. The ionic core environment is simulated by projector augmented-wave (PAW) pseudopotentials.<sup>14</sup> We use a Hubbard  $U = 4.2\text{ eV}$  on the  $3d$  orbitals of Mn and Fe.<sup>15</sup> The magnetic moments are collinear and spin-orbit coupling is neglected. The cutoff energy for all calculations is  $550\text{ eV}$ . The energy error threshold varies slightly in different calculations, but an accuracy between  $1.0 \times 10^{-5}$  and  $1.0 \times 10^{-7}\text{ eV}$  is achieved. The forces are reduced below  $0.01\text{ eV/\AA}$  in the DW structural relaxations.  $2 \times 6 \times 2$  and  $6 \times 6 \times 1$   $k$  meshes are used in the calculations of X-walls and Y-walls respectively as defined below.

## III. RESULTS AND DISCUSSION

### A. Construction of domain walls

The general structure of corundum derivatives  $\text{ABO}_3$  and  $\text{A}_2\text{BB}'\text{O}_6$  were introduced previously.<sup>11</sup> Here we only focus on the  $\text{LiNbO}_3$  (LNO)-type and ordered-LNO structures, which are compatible with ferroelectricity along the rhombohedral axis. In Fig. 1, both the rhombohedral unit cell and views from different hexagonal directions are illustrated. Each cation is in a distorted oxygen octahedron; these only fill two thirds of the octahedral sites, leaving cation-vacant positions that we denote by “—”. The FE reversal is driven by migration of each  $A$  cation from its own oxygen octahedron to the cation-vacant octahedron above or beneath it.<sup>16,17</sup> The reversal path can be qualitatively described by two variables  $\xi_1$  and  $\xi_2$  defined as the vertical distances between each  $A$  cation and the oxygen plane that it penetrates during the

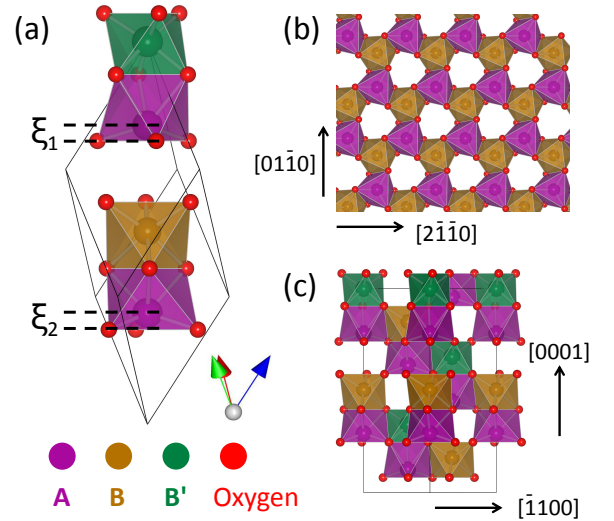


FIG. 1. Structure of ordered-LNO corundum derivatives  $\text{A}_2\text{BB}'\text{O}_6$ , and of LNO-type  $\text{ABO}_3$  corundum derivatives if  $B' = B$ . (a) Side view of the rhombohedral unit cell.  $\xi_1$  (or  $\xi_2$ ) is the vertical distance between an  $A$  cation and the oxygen plane that it penetrates during the polarization reversal. (b) Top view of the  $AB$  layer and (c) side view in the enlarged hexagonal-setting cell.

polarization reversal.<sup>11</sup> The definitions of  $\xi_1$  and  $\xi_2$  are also shown in Fig. 1(a).

In order to study the properties of DWs, we construct a supercell with a polarization-up domain and a polarization-down domain that are related by inversion through a center located in the FE DW separating them. Because of periodic boundary conditions, there are always two DWs in the supercell, one denoted as  $\text{DW}_{\uparrow\downarrow}$  (polarization up on the left and down on the right) and the other as  $\text{DW}_{\downarrow\uparrow}$  (the opposite case). In corundum derivatives the  $R3c$  symmetry of the LNO-type structure ensures that the  $\text{DW}_{\uparrow\downarrow}$  and  $\text{DW}_{\downarrow\uparrow}$  walls are equivalent, but they become inequivalent in the ordered-LNO structure with  $R3$  symmetry. Because  $\text{DW}_{\uparrow\downarrow}$  and  $\text{DW}_{\downarrow\uparrow}$  always come in pairs in our supercell calculations, we report only the average formation energy of  $\text{DW}_{\uparrow\downarrow}$  and  $\text{DW}_{\downarrow\uparrow}$  for the ordered-LNO materials.

The intrinsic difference between  $\text{DW}_{\uparrow\downarrow}$  and  $\text{DW}_{\downarrow\uparrow}$  in the ordered-LNO structure arises from the chiral nature of the structure. The ordered-LNO space group is  $R3$ , which does not contain any mirror symmetries and is therefore chiral. In contrast, the LNO-type structure is not chiral because of its  $R3c$  symmetry. The hands shown in Fig. 2 illustrate how the chirality of the FE domains implies that  $\text{DW}_{\uparrow\downarrow}$  and  $\text{DW}_{\downarrow\uparrow}$  are inequivalent. The fingers point in the polarization direction, and the left (L) or right (R) hand represents the L or R chirality. The ferroelectricity in corundum derivatives is generated by breaking the inversion symmetry from the reference structure with symmetry  $R\bar{3}$ ,<sup>11</sup> so the two FE domains with op-

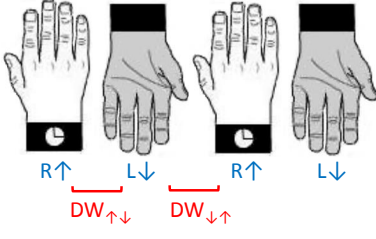


FIG. 2. Illustration of domains and DWs in ordered-LNO materials. FE DWs are formed between ( $R\uparrow$ ) domains and ( $L\downarrow$ ) domains. The DW between adjacent thumbs represents  $DW_{\uparrow\uparrow}$  and the DW between adjacent little fingers represents  $DW_{\downarrow\downarrow}$ . Left and right hands represent left (L) and right (R) chirality, and the direction in which the fingers point ( $\uparrow$  or  $\downarrow$ ) represents the polarization direction.

posite polarization are related by an inversion operation. Since the inversion operation flips both polarization and chirality, the FE DW is also a chiral DW. Such an interlocking effect between polarization and chirality at the DW was observed in chiral pyroelectric  $\text{Ni}_3\text{TeO}_6$ .<sup>10</sup> It is also clear that there are two kinds of interfaces between hands as shown in Fig. 2, one between thumbs and the other one between little fingers, and these correspond to the  $DW_{\downarrow\uparrow}$  and  $DW_{\uparrow\downarrow}$ .

The presence of this chirality can also help explain the observed shape of domains in corundum-derivative materials. In  $\text{LiNbO}_3$  and other LNO-type materials with  $R3c$  symmetry, the Wulff construction<sup>18</sup> implies that the ideal domain shape is a regular hexagon, because  $DW_{\uparrow\downarrow}$  and  $DW_{\downarrow\uparrow}$  have identical formation energies. As the asymmetry between the energies of  $DW_{\uparrow\downarrow}$  and  $DW_{\downarrow\uparrow}$  increases, the Wulff shape first distorts into an equiangular hexagon having alternating long and short sides, and eventually into a triangle in which only the favored DW is exposed. In fact, regular hexagonal domains are observed in  $\text{LiNbO}_3$ <sup>19</sup> while triangular domains are found in  $\text{Ni}_3\text{TeO}_6$  with the ordered-LNO structure.<sup>10</sup>

To arrive at our DW configurations, we assume that the  $B/B'$  and O sublattices are preserved throughout the supercell, so that the DW only results from the interchange of  $A$  and  $-$  sublattices (that is, migration of  $A$  cations into vacancies) on one side of the DW. This is motivated by the greater mobility of the  $A$  cation species. In addition, only the  $180^\circ$  charge-neutral DW is considered, in which the polarization direction is parallel to the DW plane but antiparallel between domains.

### B. Orientation of domain walls

Since corundum derivatives have three-fold symmetry, there are two types of  $180^\circ$  DWs depending on the orientation of the DW plane. We refer to a DW in the  $x$ - $z$  plane as an X-wall and one in the  $y$ - $z$  plane as a Y-wall. Top and side views of the X-wall and Y-wall are shown in

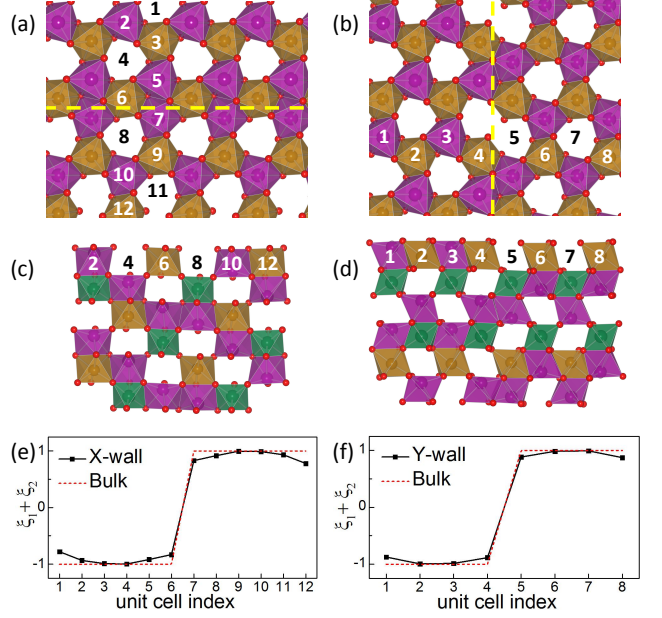


FIG. 3. Structures of the X-wall in the 6+6 supercell (left) and the Y-wall in the 4+4 supercell (right). (a,b) Top views of the X-wall and Y-wall. The number in each octahedron is the unit cell label. The X-wall lies in the  $x$ - $z$  or  $(01\bar{1}0)$  plane and is located between the 6th and the 7th unit cell as shown by the dashed yellow line. The Y-wall lies in the  $y$ - $z$  or  $(2\bar{1}\bar{1}0)$  plane and is located between the 4th and the 5th unit cell. (c,d) Side views of the X-wall and Y-wall. Odd-number cells are behind even-number cells in the X-wall. (e,f) The  $\xi_1 + \xi_2$  displacement profile of an X-wall and a Y-wall.

Fig. 3 in comparison with the bulk structure in Fig. 1(b-c). In the layer shown in Fig. 3(a), octahedra containing  $A$  cations are densely packed at the X-wall. However, there are also layers where the octahedra at the X-wall are all cation-vacant. In short, the X-wall consists of alternating dense and sparse octahedral layers. In comparison, the  $A$  and  $-$  sublattices are more evenly spaced at the Y-wall.

To calculate the formation energies, we construct 6+6 and 6+7 supercells for the X-wall, and 3+4, 4+4, and 4+5 supercells for the Y-wall. Here the supercell notation  $m + n$  means that  $m$  unit cells are of polarization down and  $n$  unit cells are of polarization up. The  $m + m$  supercell preserves some symmetry, while the  $m + (m + 1)$  supercell has none because of the asymmetry of the size of up and down domains. In the  $m + m$  supercells, the up and down domains are related by an inversion symmetry through a center lying in the DW. Furthermore, for the LNO-type structure, the identical  $DW_{\uparrow\downarrow}$  and  $DW_{\downarrow\uparrow}$  are also related by two-fold rotation. The computed relaxed displacements  $\xi_1 + \xi_2$  in each cell of the 6+6 X-wall and the 4+4 Y-wall of  $\text{Li}_2\text{ZrTeO}_6$  are shown in Fig. 3(e) and (f). The displacement profiles suggest that the DWs in corundum derivatives are atomically sharp, similar to

TABLE I. Formation energies of X-walls and Y-walls, in units of  $\text{mJ}/\text{m}^2$ . For the ordered-LNO structure, the formation energy is averaged between the  $\text{DW}_{\uparrow\downarrow}$  and  $\text{DW}_{\downarrow\uparrow}$ . The magnetic orderings are shown in the column labeled “Mag.”.

LNO-type	Mag.	X	Y	Ordered-LNO	Mag.	X	Y
$\text{LiTaO}_3$		71	63	$\text{Li}_2\text{ZrTeO}_6$		29	20
$\text{LiNbO}_3$		160	138	$\text{Li}_2\text{HfTeO}_6$		30	21
$\text{ZnSnO}_3$		106	81	$\text{Mn}_3\text{WO}_6$	<i>udu-udu</i>	68	42
$\text{MnTiO}_3$	<i>ud-ud</i>	171	153	$\text{Mn}_3\text{WO}_6$	<i>udu-dud</i>	67	41
$\text{FeTiO}_3$	<i>ud-ud</i>	183	108	$\text{Mn}_3\text{WO}_6$	<i>udu-udu</i>	75	45

the DWs of perovskites.<sup>20,21</sup> Meanwhile, our calculations also predict that the Y-wall is energetically favored in all the cases that we have studied, as shown by the converged DW formation energies in Table I. Our results for  $\text{LiNbO}_3$  and  $\text{LiTaO}_3$  are consistent with the earlier DW simulations.<sup>22</sup> Experimental observations on the domains of  $\text{LiNbO}_3$  also confirm that the Y-wall is more favorable.<sup>19</sup>

### C. Magnetic and magnetoelectric domain walls

Some corundum derivatives are magnetic compounds and exhibit magnetic order. Here we use notations like “*udu*” to represent spin-up (*u*) and spin-down (*d*) states on magnetic cations  $A_1$ ,  $A_2$  and  $B$  in that order, where  $A_1$  and  $A_2$  are face-sharing with  $B'$  and  $B$  cations respectively. Since spin-orbit coupling is neglected in our calculations, “up” and “down” are not necessarily  $\pm\hat{z}$ . In our previous work<sup>11</sup> it was shown if the magnetic order is constrained to preserve the rhombohedral unit cell, the ground state is antiferromagnetic (or *ud*) for  $\text{MnTiO}_3$  and  $\text{FeTiO}_3$ , while in  $\text{Mn}_3\text{WO}_6$  the lowest-energy state is ferrimagnetic *udu* but with *uud* close in energy.

Because of the time-reversal symmetry, a global reversal of all the spins does not affect the total energy, e.g., *udu* and *dud* have exactly the same energy in the bulk of ferrimagnetic compounds such as  $\text{Mn}_3\text{WO}_6$ . This means that there are two possibilities for the magnetic order across a FE DW: the magnetization may be the same on both sides of the DW, or it may reverse. The former case is illustrated by Case 1 in Fig. 4, and the corresponding DW is denoted by *udu-udu*. Here the letters before and after “-” represent magnetic orders in two neighboring domains. If the magnetic order reverse across the DW, as shown in Case 2 of the figure, the DW is denoted by *udu-dud*. Therefore, the *udu-dud* FE DW is also a magnetic DW. Similarly, there are also *ud-ud* DW and *ud-du* DWs for  $\text{MnTiO}_3$  and  $\text{FeTiO}_3$ , but neither of them has a net magnetization.

Our computed formation energies for both the *udu-udu* and *udu-dud* DWs are summarized in Table I. Interestingly, the results suggest that the magnetization-reversing *udu-dud* DW is energetically favored, implying

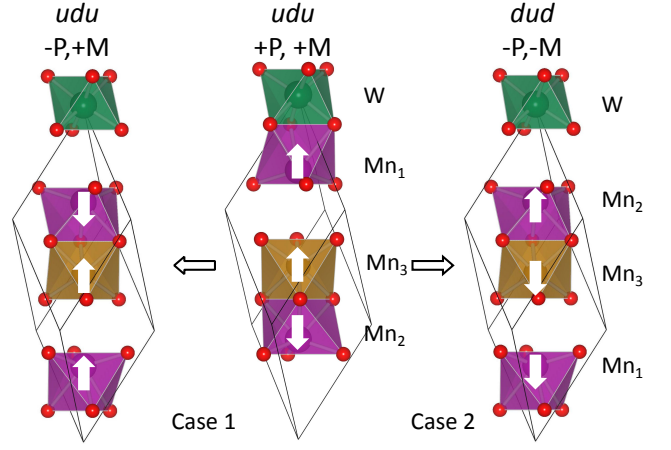


FIG. 4. Two possible magnetic orders at FE DWs in  $\text{Mn}_3\text{WO}_6$ . The structure in the center has polarization and magnetization (+P,+M) with the magnetic order *udu*. The structures on the left and right both have polarization  $-P$  but the left one has the magnetic order *udu* while the right one is *dud*. In Case 1, the FE DW is formed between structures in the center and on the left. In Case 2, the FE DW is formed by the central and rightward structures.

that the FE and magnetic domains are interlocked. This has interesting consequences. When a switching electric field is applied to a polydomain FE sample, the FE DWs move so that the favored domains grow at the expense of the unfavored ones, as illustrated in Fig. 5. Because the magnetic order reverses across the DW, the magnetization is simultaneously switched in the same process. This provides an extrinsic mechanism for magnetoelectric coupling that could have useful device implications. Other similar cases of DW-mediated interlocking of two order parameters have been discussed previously.<sup>23</sup>

As the spin-orbit coupling is not included in our calculations, the origin of the coupling between magnetization and polarization at the DW should be categorized as an exchange-striction effect. Comparing the bulk and DW structures, it is found that, for example, the *A* octahedron (purple color) is only edge sharing with three *B* oc-

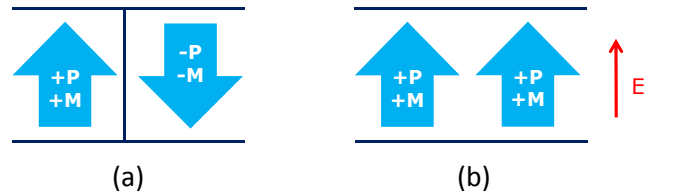


FIG. 5. Illustration of magnetoelectric coupling at FE DWs when *udu-dud* is favored. (a) Magnetization direction is coupled to the polarization direction in different FE domains. (b) When the polarization is reversed by an electric field, the magnetization reverses as well.



tahedra in Fig. 1(b), but at the Y-wall shown in Fig. 3(d), the  $A$  octahedron has an additional edge-sharing  $A$  octahedron at the DW. Therefore, the different neighbour environments lead to different exchange energies at the two kinds of DW, explaining the interlocking of magnetism and polarization.

In the above calculations, the magnetic DW is assumed to be as sharp as the FE DW. One may recall that in most magnetic materials the magnetic DWs are much broader, and wonder whether we should consider a broad magnetic DW instead. We don't believe so. In most ferromagnetic DWs, the exchange energy prefers a gradual change of spin directions at the DW, but the magnetic anisotropy favors an abrupt change of spin directions at the DW. Thus, in the case of strong exchange and weak spin anisotropy, magnetic DWs are much broader than FE DWs. However, in *udu*  $\text{Mn}_3\text{WO}_6$ , because of the distinct structure at the FE DW, the exchange energy also prefers the spins to align oppositely (*udu-dud*) across the DW. Therefore, both exchange energy and anisotropy support the sharp magnetization change at the FE DW.

#### D. Domain wall reversal

The polarization reversal at the DW is associated with DW motion. For instance, in the 4+4 supercell illustrated in Fig. 6(a), the simultaneous polarization reversal at the 1st and the 5th cells (black arrows) causes the  $\text{DW}_{\uparrow\downarrow}$  and  $\text{DW}_{\downarrow\uparrow}$  to move to the right by one unit cell. Similarly, in the 3+4 supercell shown in Fig. 6(b), the polarization reversal at the 4th cell is accompanied by the rightward motion of the  $\text{DW}_{\downarrow\uparrow}$ , and the polarization reversal at the 7th cell leads to the leftward motion of the  $\text{DW}_{\uparrow\downarrow}$ . In order to insure that the supercells before and after the DW displacement are equivalent, the  $m+m$  supercell always involves the motion of both  $\text{DW}_{\uparrow\downarrow}$  and  $\text{DW}_{\downarrow\uparrow}$ . By contrast, the  $m+(m+1)$  supercell allows just one selected DW to move. Therefore, while either type of supercell can be used to study the barriers for DW motion in LNO-type materials, only the  $m+(m+1)$  supercells are suitable for obtaining the corresponding information about  $\text{DW}_{\uparrow\downarrow}$  and  $\text{DW}_{\downarrow\uparrow}$  walls separately in the ordered-LNO case.

The adiabatic polarization reversal at the DW is achieved by using the reaction coordinate  $\xi_1 + \xi_2$  as a structural constraint<sup>11</sup> and applying it only to the unit cell at the DW. The energy profiles of the DW-mediated reversal of selected materials are illustrated in Fig. 6(d), and the reversal barriers are listed in Table. II. This DW-mediated barrier is much lower in energy than the coherent reversal barrier reported in our previous work.<sup>11</sup> For instance, the coherent barrier of  $\text{LiTaO}_3$  is 129 meV while the DW-mediated barrier is only 55 meV. This huge energy reduction is caused by the distinct structure at the DW. Since the symmetry at the DW is much lower than in the bulk, there are more phonon modes, e.g., the breathing modes of the oxygen triangle, that can undergo

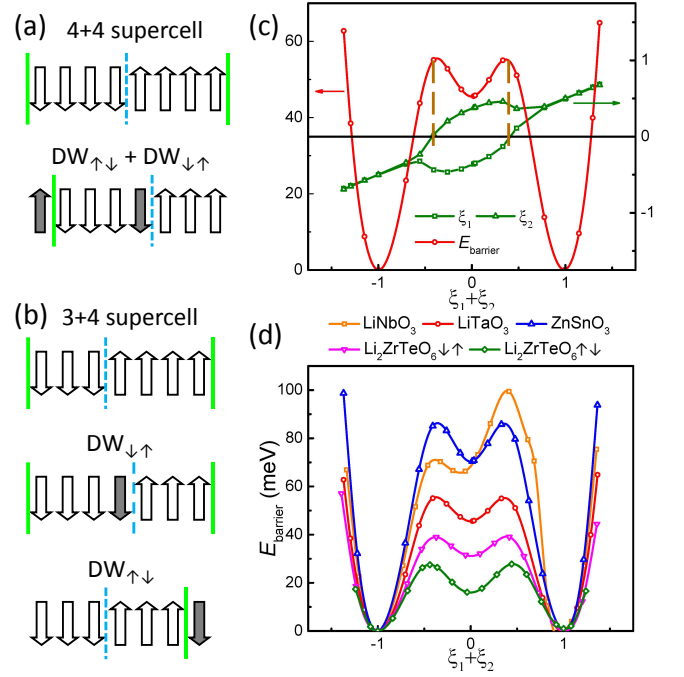


FIG. 6. DW-mediated FE reversal in corundum derivatives. (a-b) Illustrations of DW motions in 4+4 and 3+4 supercells. The upward and downward arrows represent the polarization in each unit cell. The dashed blue line represents the  $\text{DW}_{\downarrow\uparrow}$  and the solid green line is the  $\text{DW}_{\uparrow\downarrow}$ . The filled black arrows represent the polarization that is reversed during the DW motion. (c) Energy profile of the DW reversal in  $\text{LiTaO}_3$  and the evolution of  $\xi_1$  and  $\xi_2$ . The dashed brown lines highlight the positions where  $\xi_1 = 0$  and  $\xi_2 = 0$ . (d) Energy profiles of the DW reversal for selected corundum derivatives. The results of both the  $\text{DW}_{\downarrow\uparrow}$  and  $\text{DW}_{\uparrow\downarrow}$  are included for  $\text{Li}_2\text{ZrTeO}_6$ . Energy units are meV per unit cell.

displacement to lower the energy barrier. In addition, the DW-mediated reversal paths are insulating in all the cases that we have calculated including that of  $\text{FeTiO}_3$ , which we reported to have a conducting coherent reversal path in our previous calculations.<sup>11</sup>

The energy profiles shown in Fig. 6(d) are symmetric with respect to  $\xi_1 + \xi_2 = 0$  for most candidates, as their DW structures have inversion symmetry at  $\xi_1 + \xi_2 = 0$ . The only asymmetric profile in Fig. 6(d) is that of  $\text{LiNbO}_3$ . This is caused by an in-plane unstable polar mode at the midpoint structure, which breaks the local inversion symmetry at  $\xi_1 + \xi_2 = 0$ . This unstable  $E_u$  mode in  $\text{LiNbO}_3$  has been previously reported in the literature.<sup>11,17</sup>

In Fig. 6(c), we use the results for  $\text{LiTaO}_3$  as an example to clarify the relationship between the energy profile and the evolution of  $\xi_1$  (or  $\xi_2$ ) at the DW. Similar to the results in our previous work,<sup>11</sup>  $\xi_1 \neq \xi_2$  when the reaction coordinate  $\xi_1 + \xi_2$  approaches zero, which means that the two  $A$  cations do not migrate simultaneously. However, the barrier structures for the DW-mediated reversal are

TABLE II. DW-mediated polarization reversal barriers  $E_{\text{barrier}}$  for corundum derivatives. The energy barriers of  $\text{DW}_{\uparrow\downarrow}$  and  $\text{DW}_{\downarrow\uparrow}$  are the same in the LNO-type structure, but different in the ordered-LNO structure. Energy units are meV per unit cell.

LNO-type	Mag.	$\uparrow\downarrow=\downarrow\uparrow$	Ordered LNO	Mag.	$\uparrow\downarrow$	$\downarrow\uparrow$
LiTaO <sub>3</sub>		55	Li <sub>2</sub> ZrTeO <sub>6</sub>		28	39
LiNbO <sub>3</sub>		98	Li <sub>2</sub> HfTeO <sub>6</sub>		32	42
ZnSnO <sub>3</sub>		86	Mn <sub>3</sub> WO <sub>6</sub>	<i>udu-udu</i>	210	161
MnTiO <sub>3</sub>	<i>ud-ud</i>	229	Mn <sub>3</sub> WO <sub>6</sub>	<i>udu-dud</i>	212	181
FeTiO <sub>3</sub>	<i>ud-ud</i>	394	Mn <sub>3</sub> WO <sub>6</sub>	<i>udu-udu</i>	207	175

qualitatively different from those for the coherent reversal, where the energy profile displayed a single maximum at  $\xi_1 + \xi_2 = 0$  in most cases.<sup>11</sup> In contrast, the DW-mediated energy profile has two energy maxima located at approximately  $\xi_1 = 0$  and  $\xi_2 = 0$ , as highlighted by the dashed vertical lines in Fig. 6(c). Each of these configurations corresponds to the moment when one of the  $A$  cations passes through an oxygen plane.

For magnetic compounds, their DW motions may be accompanied by spin flips at the DWs. In the reversal process, the  $A_1$  cation migrates away from the  $B'$  cation and becomes face sharing with the  $B$  cation. Similarly, the  $A_2$  cation moves away from the  $B$  cation and forms face-sharing octahedra with the  $B'$  cation. This can result in a change of the magnetic order, as for example in Mn<sub>3</sub>WO<sub>6</sub> where the *udu* magnetic order becomes *dud* as  $A_1$  interchanges with  $A_2$ . In order to arrive at the magnetic ground state, either the spins on both  $A_1$  and  $A_2$  cations have to flip so that *dud* becomes *udu*, or the spin on the  $B$  cation has to flip so that *dud* becomes *dud*. The former case happens at the *udu-udu* DW, and the latter case happens at the *udu-dud* DW.

The above-mentioned first-principles methods can be used to predict the DW-mediated reversal barrier in any corundum derivative, but it would be more valuable if some intuitive rules of thumb can be summarized to enhance our understanding. In the discussion of the polar metal LiOsO<sub>3</sub>, which is also a corundum derivative, it has been pointed out that the polar distortion is driven by short-range interactions,<sup>24</sup> or from the crystal chemistry point of view, it is caused by the local bonding preference of Li cations.<sup>25</sup> As the Li cations are loosely bonded in the centrosymmetric structure, they prefer a polar distortion to strengthen the local bonding environment. Because of the structural similarity between metallic LiOsO<sub>3</sub> and other insulating corundum derivatives, it is worth investigating the relationship between the bonding environment of the  $A$  cations and the DW-mediated reversal barrier.

The local bonding of the  $A$  cation can be described by the empirical bond valence sum (BVS) through the equation<sup>26</sup>

$$V_{\text{BVS}} = \sum_i \exp[(R_0 - R_i)/b]. \quad (1)$$

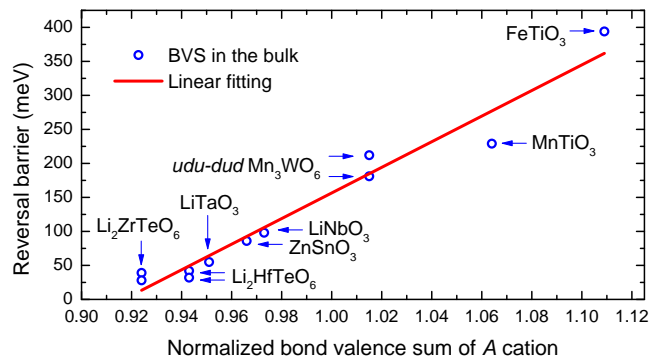


FIG. 7. Scatterplot of DW-mediated reversal barrier *versus* normalized  $A$ -cation bond valence sum (i.e., divided by valence charge). The linear fit is of the form  $y = a + b(x - 1)$  with  $a = 157$  meV and  $b = 1883$  meV.

$V_{\text{BVS}}$  estimates the number of electrons that are associated with the local bonds. Here  $R_i$  is the bond length between  $A$  cations and the  $i$ th nearest neighboring oxygen anions,  $R_0$  is a tabulated parameter expressing the ideal bond length when  $V_{\text{BVS}}$  is exactly equal to the valence of the  $A$  cation and  $b$  is an empirical constant 0.37 Å. For ordered-LNO structures, the two  $A$  cations are inequivalent. Instead of using the average  $V_{\text{BVS}}$  of two  $A$  cations, it is more relevant to only consider the  $A$  cation that is closer to the oxygen plane, because that is the one that would migrate first in the reversal process. Using the bond-length values extracted from bulk structures and Eq. (1), we plot the energy barrier *versus* the normalized  $V_{\text{BVS}}$  in Fig. 7. A roughly linear relationship is observed between the normalized  $V_{\text{BVS}}$  of the  $A$  cations and the DW-mediated reversal barriers, which also implies the dominance of short-range interactions in the corundum derivatives. The bond valence model is also the basis of empirical interatomic potentials that have been successfully used for molecular dynamics simulations of ferroelectric perovskites such as PbTiO<sub>3</sub>.<sup>27</sup>

#### IV. SUMMARY AND OUTLOOK

A DW is a topological defect that may exhibit rich physics not present in the bulk. FE DWs separate two polar domains. In this work, we have studied the properties of FE DWs in corundum derivatives. The mobile 180° charged-neutral DWs are constructed by interchanging  $A$ -cation and vacancy sublattices while preserving the  $B/B'$  and O sublattices. Interestingly, it is found that the mobile FE domains are interlocked with chirality domains, so that the FE DW is also a chiral DW. For the orientation of DWs, our calculations suggest that the  $Y$ -wall lying in the  $y$ - $z$  plane is more stable than the  $X$ -wall lying in the  $x$ - $z$  plane.

We have also considered the magnetic order at the DW, and found that in Mn<sub>3</sub>WO<sub>6</sub> with *udu* magnetic order, the

domains with opposite polarization also have opposite magnetization, as controlled by exchange-striction interactions at the DW. Therefore both the polarization and magnetization can be controlled by an electric field. We note that the magnetic structure of  $\text{Mn}_3\text{WO}_6$  is still under investigation,<sup>28</sup> and it is possible that the actual magnetic structure has a larger magnetic cell as in  $\text{Ni}_3\text{TeO}_6$ , or even a non-collinear magnetic order, instead of our assumed collinear *udu* magnetic order. Nevertheless, we expect that this kind of DW-mediated magnetoelectric coupling may still exist in the presence of a more complicated magnetic order, or in other magnetic corundum derivatives.

Since the FE polarization reversal is achieved through DW motion, we have also studied the DW-mediated polarization reversal pathways and barriers by applying structural constraints at the DW. We found that the DW-mediated reversal barrier is approximately linearly correlated with the bond valence sum of the *A* cations.

Since the local bonding environment is accessible to experiment, this linear relationship can provide a useful rule of thumb in predicting the DW-mediated reversal barrier of potential new FE materials of this class.

Finally, we note that there are other classes of DWs, such as purely chiral DWs or simultaneously chiral and magnetic DWs, that may occur in these materials. Although not relevant for FE switching, such domain walls might have other interesting properties that would be worth investigating.

## V. ACKNOWLEDGMENT

We thank Sang-Wook Cheong and Weida Wu for their insightful suggestions. The work was supported by ONR grant N00014-12-1-1035.

- 
- \* mengye@physics.rutgers.edu
- <sup>1</sup> Karin M. Rabe, Charles H Ahn, and Jean-Marc Triscone, *Physics of Ferroelectrics*, 1st ed., Vol. 105 (Springer-Verlag Berlin Heidelberg, 2007).
  - <sup>2</sup> P. Muralt, “Ferroelectric thin films for micro-sensors and actuators: a review,” *Journal of Micromechanics and Microengineering* **10**, 136 (2000).
  - <sup>3</sup> James F. Scott, *Ferroelectric Memories*, 1st ed., Vol. 3 (Springer-Verlag Berlin Heidelberg, 2000).
  - <sup>4</sup> Lixin He and David Vanderbilt, “First-principles study of oxygen-vacancy pinning of domain walls in  $\text{PbTiO}_3$ ,” *Phys. Rev. B* **68**, 134103 (2003).
  - <sup>5</sup> Jan Seidel, Lane W Martin, Q He, Q Zhan, Y-H Chu, A Rother, ME Hawkrigde, P Maksymovych, P Yu, M Gajek, *et al.*, “Conduction at domain walls in oxide multiferroics,” *Nature Materials* **8**, 229–234 (2009).
  - <sup>6</sup> SY Yang, J Seidel, SJ Byrnes, P Shafer, C-H Yang, MD Rossell, P Yu, Y-H Chu, JF Scott, JW Ager, *et al.*, “Above-bandgap voltages from ferroelectric photovoltaic devices,” *Nature nanotechnology* **5**, 143–147 (2010).
  - <sup>7</sup> Yoon Seok Oh, Xuan Luo, Fei-Ting Huang, Yazhong Wang, and Sang-Wook Cheong, “Experimental demonstration of hybrid improper ferroelectricity and the presence of abundant charged walls in  $(\text{Ca,Sr})_3\text{Ti}_2\text{O}_7$  crystals,” *Nature Materials* **14**, 407–413 (2015).
  - <sup>8</sup> T Choi, Y Horibe, HT Yi, YJ Choi, Weida Wu, and S-W Cheong, “Insulating interlocked ferroelectric and structural antiphase domain walls in multiferroic  $\text{YMnO}_3$ ,” *Nature Materials* **9**, 253–258 (2010).
  - <sup>9</sup> Yanan Geng, Nara Lee, YJ Choi, S-W Cheong, and Weida Wu, “Collective magnetism at multiferroic vortex domain walls,” *Nano Letters* **12**, 6055–6059 (2012).
  - <sup>10</sup> Xueyun Wang, Fei-Ting Huang, Junjie Yang, Yoon Seok Oh, and Sang-Wook Cheong, “Interlocked chiral/polar domain walls and large optical rotation in  $\text{Ni}_3\text{TeO}_6$ ,” *APL Materials* **3**, 076105 (2015).
  - <sup>11</sup> Meng Ye and David Vanderbilt, “Ferroelectricity in corundum derivatives,” *Phys. Rev. B* **93**, 134303 (2016).
  - <sup>12</sup> G. Kresse and J. Furthmüller, “Efficient iterative schemes for *ab initio* total-energy calculations using a plane-wave basis set,” *Phys. Rev. B* **54**, 11169–11186 (1996).
  - <sup>13</sup> John P. Perdew, Adrienn Ruzsinszky, Gábor I. Csonka, Oleg A. Vydrov, Gustavo E. Scuseria, Lucian A. Constantin, Xiaolan Zhou, and Kieron Burke, “Restoring the density-gradient expansion for exchange in solids and surfaces,” *Phys. Rev. Lett.* **100**, 136406 (2008).
  - <sup>14</sup> P. E. Blöchl, “Projector augmented-wave method,” *Phys. Rev. B* **50**, 17953–17979 (1994).
  - <sup>15</sup> S. L. Dudarev, G. A. Botton, S. Y. Savrasov, C. J. Humphreys, and A. P. Sutton, “Electron-energy-loss spectra and the structural stability of nickel oxide: An LSDA+U study,” *Phys. Rev. B* **57**, 1505–1509 (1998).
  - <sup>16</sup> Iris Inbar and R. E. Cohen, “Comparison of the electronic structures and energetics of ferroelectric  $\text{LiNbO}_3$  and  $\text{LiTaO}_3$ ,” *Phys. Rev. B* **53**, 1193–1204 (1996).
  - <sup>17</sup> M. Veithen and Ph. Ghosez, “First-principles study of the dielectric and dynamical properties of lithium niobate,” *Phys. Rev. B* **65**, 214302 (2002).
  - <sup>18</sup> Paul Groth, *Zeitschrift für Kristallographie und Mineralogie*, Vol. 11 (Wilhelm Engelmann, 1893).
  - <sup>19</sup> Donghwa Lee, Haixuan Xu, Volkmar Dierolf, Venkatraman Gopalan, and Simon R. Phillpot, “Shape of ferroelectric domains in  $\text{LiNbO}_3$  and  $\text{LiTaO}_3$  from defect/domain-wall interactions,” *Applied Physics Letters* **98**, 092903 (2011), 10.1063/1.3560343.
  - <sup>20</sup> J. Padilla, W. Zhong, and David Vanderbilt, “First-principles investigation of  $180^\circ$  domain walls in  $\text{BaTiO}_3$ ,” *Phys. Rev. B* **53**, R5969–R5973 (1996).
  - <sup>21</sup> B. Meyer and David Vanderbilt, “*Ab initio* study of ferroelectric domain walls in  $\text{PbTiO}_3$ ,” *Phys. Rev. B* **65**, 104111 (2002).
  - <sup>22</sup> Donghwa Lee, Haixuan Xu, Volkmar Dierolf, Venkatraman Gopalan, and Simon R. Phillpot, “Structure and energetics of ferroelectric domain walls in  $\text{LiNbO}_3$  from atomic-level simulations,” *Phys. Rev. B* **82**, 014104 (2010).
  - <sup>23</sup> Nicole A. Benedek and Craig J. Fennie, “Hybrid improper ferroelectricity: A mechanism for controllable polarization-

- magnetization coupling,” *Phys. Rev. Lett.* **106**, 107204 (2011).
- <sup>24</sup> Pengfei Li, Xinguo Ren, Guang-Can Guo, and Lixin He, “The origin of hyperferroelectricity in  $\text{LiBO}_3$  ( $B = \text{V}, \text{Nb}, \text{Ta}, \text{Os}$ ),” *Scientific Reports* **6**, 34085 (2016).
- <sup>25</sup> Nicole A Benedek and Turan Birol, “‘Ferroelectric’ metals reexamined: Fundamental mechanisms and design considerations for new materials,” *Journal of Materials Chemistry C* **4**, 4000–4015 (2016).
- <sup>26</sup> I. D. Brown and D. Altermatt, “Bond-valence parameters obtained from a systematic analysis of the Inorganic Crystal Structure Database,” *Acta Crystallographica Section B* **41**, 244–247 (1985).
- <sup>27</sup> Young-Han Shin, Valentino R. Cooper, Ilya Grinberg, and Andrew M. Rappe, “Development of a bond-valence molecular-dynamics model for complex oxides,” *Phys. Rev. B* **71**, 054104 (2005).
- <sup>28</sup> Private communication with Prof. Martha Greenblatt and Dr. Manrong Li.